

Published in final edited form as:

Lab Chip. 2012 April 21; 12(8): 1427–1430. doi:10.1039/c2lc21225k.

Cell sorting by deterministic cell rolling†‡

Sungyoung Choi^a, Jeffrey M. Karp^b, and Rohit Karnik^a

^aDepartment of Mechanical Engineering, Massachusetts Institute of Technology, Cambridge, MA, 02139. karnik@mit.edu; Fax: +617-258-9346; Tel: +617-324-1155

^bDivision of Biomedical Engineering, Department of Medicine, Center for Regenerative Therapeutics, Brigham and Women's Hospital, Harvard Medical School, Harvard Stem Cell Institute, Harvard-MIT Division of Health Sciences and Technology, Cambridge, MA, 02139. jkarp@rics.bwh.harvard.edu; Fax: +617-768-8338; Tel: +617-817-9174

Abstract

This communication presents the concept of “deterministic cell rolling”, which leverages transient cell-surface molecular interactions that mediate cell rolling to sort cells with high purity and efficiency in a single step.

Separation of specific populations of cells from a heterogeneous mixture constitutes an important process in biomedical research, regenerative medicine, and cell-based diagnostics.¹ Cells can be identified by their intrinsic biophysical characteristics such as morphology, size, density, and dielectric or magnetic susceptibility.^{2–5} Sorting based on these properties is label-free, but often lacks specificity. Alternatively, cells can be sorted based on specific biological markers. Such methods include fluorescence-activated cell sorting (FACS) and magnetic-activated cell sorting (MACS), or capture on affinity molecule-coated surfaces. The use of labels, however, introduces labeling and label-removal steps and can produce unintended adverse effects on the cellular phenotype.⁶ Affinity columns and affinity capture in microfluidic devices enable label-free separation in which target cells can be captured and recovered by elution.^{7–11} This approach has demonstrated good performance in sorting of CD34⁺ cells using CD34 antibody,⁷ CD4⁺ T-lymphocytes using CD4 antibody,⁸ CD34⁺ haematopoietic stem and progenitor cells using P-selectin (CD62P),⁹ breast cancer cells using E-selectin (CD62E),¹⁰ and circulating tumor cells (CTCs) using epithelial cell adhesion molecule (EpCAM, CD326)¹¹ among other applications. Compared to affinity columns, microfluidic devices enable better flow control and visualization. To improve the process of affinity separation, microfluidic devices have also employed mixing approaches using surface grooves to create circulating streamlines¹² that enhance cell-surface interactions, resulting in higher capture efficiency of CTCs.¹¹ In these approaches, the number of cells that can be captured is limited by the surface area coated with affinity molecules that often determines the cost of the device. In addition, release of the captured cells for culture, enumeration, or analysis comprises an additional non-trivial step.

†Conflict-of-interest disclosure: J.M.K. is a co-owner of Megacell Therapeutics, a company that has an option to license IP generated by J.M.K. J.M.K. may benefit financially if the IP is licensed and further validated. The interests of J.M.K. were reviewed and are subject to a management plan overseen by the Brigham & Women's Hospital and Partners HealthCare in accordance with their conflict of interest policies.

‡Electronic supplementary information (ESI) available: Experimental section; Supplemental discussion; two movies illustrating deterministic cell rolling and sorting. See DOI: 10.1039/c2lc21225k

© The Royal Society of Chemistry 2012

The remaining authors declare no competing financial interests.

We describe a new separation process called “deterministic cell rolling” that combines transient cell–surface molecular interactions with passive hydrodynamic control to separate cells in a continuous process without requiring separate capture and elution steps. Such transient cell-surface interactions occur in a physiological phenomenon known as cell rolling, which involves continuous formation and dissociation of cell-surface adhesive bonds under fluid flow. Cell rolling plays an important role in the trafficking of lymphocytes, platelets, hematopoietic stem and progenitor cells, and metastatic cancer cells.^{10,13,14} The device for deterministic cell rolling consists of easily parallelizable microfluidic channels with three-dimensional topography that work in synergy to induce effective contact of cells with affinity surfaces that support rolling of target cells, which alters their trajectories and results in cell separation (Fig. 1). While researchers have investigated the possibility of sorting cells based on cell rolling, current methods require surface patterning or micro-grooves, and rely on gravitational settling for cell-surface interactions that requires a larger device footprint and yields a low throughput.¹⁵ Compared to these approaches, deterministic cell rolling enables a significantly higher efficiency of separation and a compact form factor that facilitates easy parallelization of sorting channels to process large sample volumes. Here, we demonstrate the utility of deterministic cell rolling for sorting cells based on a surface marker in a label-free, gentle, and scalable manner.

The separation principle relies on two hydrodynamic phenomena – cell rolling and hydrophoresis. For passive cell manipulation we placed slant ridges on the channel floor, which alter the streamlines and induce repeated collisions between cells and the ridges (Fig. 1).¹⁶ The slant ridges superpose a circulating flow pattern on the axial flow. In the trenches between the ridges, the flow circulates towards the sorting/gutter side of the channel, whereas in the gap above the top surface of the ridges, the flow re-circulates back towards the focusing side of the channel (Fig. S1). This recirculating flow moves downward near the focusing side of the channel, pushing the cells against the ridges (Fig. 1A, top). The size of the cells prevents them from approaching the ridges more closely than the cell radius. In the case of non-target cells that do not roll on the ridges, this interaction forces the cells to remain above the ridges in the gap region where the flow converges towards the focusing side of the channel. These physical interactions result in self-ordering of non-target cells on the focusing side (Fig. 1A). The non-target cells thus follow a trajectory (the dotted arrow in Fig. 1A, bottom right) that keeps them out of the trench (the solid arrow in Fig. 1A, bottom right). This effect is called hydrophoresis.¹⁶ However, in the presence of adhesion molecules on the surfaces, target cells are forced into contact with the ridges, and as a consequence, tether (*i.e.* initiate molecular interactions) and roll on the top surface of the ridges. Upon encountering the corner of the ridges, these cells remain attached to the ridge surface and enter the trenches between the ridges where the flow circulates away from the focusing side (Fig. 1A, bottom left). Thus, the molecular forces exerted on the interacting target cells as they round the corners of the ridges nudge them into a different, laterally diverging trajectory. These cells roll along the trench and finally come out of the ridge region into the gutter region and flow onward towards the sorting exit.

For scalable parallelization, the microfluidic device was fabricated in a multilayer structure in which multiple sorting layers can be sandwiched between the top injection layer and the bottom collection layer (Fig. 1 and S2). Each sorting layer comprised ten polydimethylsiloxane (PDMS) microchannels with two sets of slant ridges (Fig. 1 and S3). The first set of ridges, called focusing ridges (FR), were designed in a narrow channel (110 μm in width), such that they can be coated with adhesion molecules, yet not support stable cell rolling due to the high shear stress (30 to 45 dyn/cm^2) (Fig. S4). The second set, called sorting ridges (SR), were designed in a wider channel (670 μm in width) that allowed stable rolling of target cells on the SR due to lower shear stress (2.5 to 3.5 dyn/cm^2). The ridges were arranged in order of decreased widths by 5 μm (from 640 μm to 385 μm), which

formed a gutter and prevented sorted cells from re-entering the ridge region. Details of the device fabrication, geometry, and experimental setup are provided in Supplementary Information.

To validate the separation principle we used leukemia cell lines with known receptor-ligand pairs for cell rolling – HL60 as a target cell, K562 as a non-target cell, and P-selectin as a specific ligand. The device was incubated with P-selectin solution ($1.5 \mu\text{g mL}^{-1}$, unless specified) at room temperature. HL60 cells express high levels of P-selectin glycoprotein ligand-1 (PSGL-1, CD62P) and exhibit rolling on P-selectin mediated primarily by PSGL-1.¹⁷ In contrast, K562 cells that lack PSGL-1 do not bind to P-selectin.^{18,19} The rolling process of HL60 cells was highly deterministic, in which the cells were forced to contact and tether on the top surface of the sorting ridges (0 s), rolled along the trench, and were finally detached and re-suspended in the gutter region (66 s) (Fig. 2A and Movie S1). Since the trajectories of the rolling and non-rolling cells differed at the corners of the ridges, we examined the flow of cells when they encountered a square post to better understand this difference. Numerical simulations suggest that the flow streamlines experienced by a cell as it approaches the corner of a ridge are similar to those near the corner of the square post (Fig. 2 and S5). The rolling cells experience shear-induced force, F_s and torque T_s , which can be estimated in the low shear regime and no-slip boundary condition as $F_s = 1.7 \times (6\pi\mu r^2 S)$ and $T_s = 0.944 \times (4\pi\mu r^3 S)$, respectively, where μ is the viscosity, r is the cell radius and S is the shear rate.²⁰ T_s is induced by F_s as the rolling cells pivot around bond clusters. We hypothesize that when the cell reaches the corner, this torque pivots the cell onto the downstream surface of the square post or the ridge. Indeed, we observed that the cells rolled around the corner of the square post and continued to roll towards the stagnation point before detaching from the surface (Fig. 2B, left). Without cell-surface interactions, the cells just followed the streamlines corresponding to the center of the cell,²¹ although they came into contact with the square post (Fig. 2B, right). These observations demonstrate that molecular interactions between the target cells and the surface exert a torque T_s that can sustain rolling over the surfaces around a right angle corner.

The location of cell tethering, *i.e.* initialization of molecular interactions, depends on the position where the cells are first focused and encounter the ridges. We observed that the majority (~56%) of the cell tethering events occurred where cells in suspension just reached the focused position (Fig. 3 and S6). This means that the steric collisions clearly occurred in the sorting channel as experimentally observed before¹⁶ and induced effective tethering of target cells on the sorting ridges. In the upstream focusing channel, all the cells are focused and assume similar trajectories (Fig. 3A). Although the cell stream spreads slightly upon entering the wider sorting channel, this upstream focusing resulted in some tethering events (~19%) on the first four sorting ridges (Fig. 3B and S6), while the remaining cells tethered further downstream. Some of the cells that tethered on the channel ceiling above the first few ridges rolled toward the focusing side (Fig. 3B), where they entered the trench and were sorted to the gutter side.

We first tested the sorting capability of the device under various operational conditions (*i.e.* shear stress, selectin concentration, and ridge angle) for an input stream comprising only HL60 or K562 cells (Fig. 4 and Fig. S7). For a single channel, we defined the sorting efficiency, $\eta_s = n_A / (n_A + n_B) \times 100$ (%), where n_A and n_B are the numbers of cells per unit time (counted at the sorting bifurcation shown in Fig. 4B) flowing to the sorting outlet A and outlet B, respectively. Increasing flow rates create higher levels of shear stress that make it difficult to sustain cell rolling,²² resulting in a decrease in the sorting efficiency at higher flow rates (Fig. 4A). In contrast, increasing P-selectin concentration (from $0.9 \mu\text{g mL}^{-1}$ to $1.5 \mu\text{g mL}^{-1}$) facilitates tethering and rolling, thereby improving the sorting efficiency (Fig. 4A). However, a further increase in the concentration to $4.0 \mu\text{g mL}^{-1}$ induced an

undesirable transition from stable rolling to firm adhesion. As a negative control, the device was blocked with 1% BSA solution (no P-selectin) and a mixture of HL60 and K562 cells was injected into the device. In this case, there were no observable cell-surface interactions and the cells were not sorted (Fig. 4A).

As such, cell rolling requires a delicate balance between rapid formation and rapid dissociation of adhesive bonds. This dynamic nature results in a trade-off between the sorting efficiency and throughput. If the flow rate is increased for achieving higher throughput, the forces and torques imposed on rolling cells accelerate bond dissociation and the cells can detach into the fluid stream without separation. Our device circumvented this limitation by employing scalable parallelization (Fig. 1B). The simple, passive channel design enables the sorting throughput to be greatly augmented by stacking multiple sorting layers without compromising performance parameters such as purity and recovery.

Next, we examined the ability of the parallel channel device to separate cells from a heterogeneous mixture. Cells were injected at a concentration of $\sim 2.4 \times 10^5$ cells mL⁻¹ (HL60 and K562 in ratio of 2:3) and a sample throughput of 70 $\mu\text{L min}^{-1}$ ($\sim 10^6$ cells h⁻¹) corresponding to a wall shear stress of 3.4 dyn/cm². The P-selectin incubation concentration was 1.5 $\mu\text{g mL}^{-1}$. For a single sorting channel, these conditions yielded $\eta_s = 89.6 \pm 4.8\%$ and $0.4 \pm 0.3\%$ for HL60 and K562 cells, respectively (Fig. 4A). A single run through the parallel channel device produced high-purity cell populations at the outlets; the outlet A with a flow rate of $\approx 51.5 \mu\text{L min}^{-1}$ held $95.0 \pm 2.8\%$ HL60 cells, while the outlet B with a flow rate of $\approx 18.9 \text{ mL min}^{-1}$ had $94.3 \pm 0.9\%$ K562 cells ($n = 5$ different devices; Fig. 4C, and Movie S2). The HL60 cells and K562 cells were enriched by factors of 28 and 11 at the corresponding outlets, respectively. The enrichment was calculated as the ratio of the numbers of HL60 cells to K562 cells (or *vice versa*) collected at the outlet, divided by the same ratio at the inlet. The sorting process yielded considerably high sorting recovery of $87.2 \pm 76.7 \pm 14.2\%$ for K562 and 3.7% and HL60 cells, respectively. Sorting recovery was calculated as the number of collected target cells in each outlet (HL60 for the outlet A and K562 for the outlet B) divided by the total number of each cell type injected. Cell loss occurred by gravitational cell settling in the injection syringe and tubing, and with cells remaining in the sorting channels and dead volumes of the collection channels. Recovery may be enhanced by using density-matched or viscous buffer solutions, or by selectively coating only the sorting channels with P-selectin. As determined by trypan blue staining, there was no significant difference between the viabilities of sorted cells ($97.4 \pm 2.6\%$ for HL60 and $96.3 \pm 3.3\%$ for K562) and unsorted cells ($97.3 \pm 2.4\%$).

In summary, deterministic cell rolling represents a new method of affinity cell separation, enabling effective cell capture, easy cell recovery, and highly scalable parallelization in a passive device. The method obviates separate capture and elution steps, and produces high-purity output streams of target and non-target cells from a single input stream of cells. The device can be configured to perform positive selection from heterogeneous cultures to enrich cells with more robust rolling capacity for therapeutic use. Many cell types including leukocytes, platelets, hematopoietic stem and progenitors, and metastatic cancer cells exhibit rolling adhesion on vascular surfaces. This approach could potentially be applied to sort cells based on these cell rolling interactions. An intriguing possibility is the design of surfaces to produce cell rolling behavior based on specific cell surface markers or phenotypes, which is so far an unexplored area. Finally, the purity and throughput may be further improved for each target cell type *via* optimization of the obstacle geometry to enhance cell-surface interactions while minimizing sorting of non-target cells, and by configuring the sorting channels in series. We therefore believe that this approach could represent a promising tool for applications including point-of-care diagnostics, cell-based therapeutics, and cell separation in research laboratories.

Supplementary Material

Refer to Web version on PubMed Central for supplementary material.

Acknowledgments

This work was supported by National Institutes of Health grants HL-095722 and HL-097172 (J.M.K.), and in part by NSF CAREER award 0952493 through the Chemical and Biological Separations program (R.K.) and the Deshpande Center for Technological Innovation at MIT. S. C. acknowledges support from the National Research Foundation of Korea Grant funded by the Korean Government NRF-2010-D00021. Devices were fabricated in the Microsystems Technology Laboratory at MIT.

Notes and references

1. Didar TF, Tabrizian M. *Lab Chip*. 2010; 10:3043. [PubMed: 20877893] Pamme N. *Lab Chip*. 2007; 7:1644. [PubMed: 18030382]
2. Chabert M, Viovy J-L. *Proc. Natl. Acad. Sci. U. S. A.* 2008; 105:3191. [PubMed: 18316742]
3. Godin M, Delgado FF, Son S, Grover WH, Bryan AK, Tzur A, Jorgensen P, Payer K, Grossman AD, Kirschner MW, Manalis SR. *Nat. Methods*. 2010; 7:387. [PubMed: 20383132]
4. Shim S, Gascoyne P, Noshari J, Hale KS. *Integr. Biol.* 2011; 3:850.
5. Kose AR, Fischer B, Mao L, Koser H. *Proc. Natl. Acad. Sci. U. S. A.* 2009; 106:21478. [PubMed: 19995975]
6. Bulte JWM, Kraitchman DL, Mackay AM, Pittenger MF, Arbab AS, Yocum GT, Kalish H, Jordan EK, Anderson SA, Khakoo AY, Read EJ, Frank JA. *Blood*. 2004; 104:3410. [PubMed: 15525839]
7. Kumar A, Srivastava A. *Nat. Protoc.* 2010; 5:1737. [PubMed: 21030950]
8. Wang K, Marshall MK, Garza G, Pappas D. *Anal. Chem.* 2008; 80:2118. [PubMed: 18288818]
9. Wojciechowski JC, Narasipura SD, Charles N, Mickelsen D, Rana K, Blair ML, King MR. *Br. J. Haematol.* 2008; 140:673. [PubMed: 18218048]
10. Myung JH, Gajjar KA, Pearson RM, Launier CA, Eddington DT, Hong S. *Anal. Chem.* 2011; 83:1078. [PubMed: 21207944]
11. Stott SL, Hsu C-H, Tsukrov DI, Yu M, Miyamoto DT, Waltman BA, Rothenberg SM, Shah AM, Smas ME, Korir GK, Floyd FP Jr, Gilman AJ, Lord JB, Winokur D, Springer S, Irimia D, Nagrath S, Sequist LV, Lee RJ, Isselbacher KJ, Maheswaran S, Haber DA, Toner M. *Proc. Natl. Acad. Sci. U. S. A.* 2010; 107:18392. [PubMed: 20930119] Wang S, Liu K, Liu J, Yu ZT-F, Xu X, Zhao L, Lee T, Lee EK, Reiss J, Lee Y-K, Chung LWK, Huang J, Rettig M, Seligson D, Duraiswamy KN, Shen CK-F, Tseng H-R. *Angew. Chem., Int. Ed.* 2011; 50:3084.
12. Stroock AD, Dertinger SKW, Ajdari A, Mezić I, Stone HA, Whitesides GM. *Science*. 295:647. [PubMed: 11809963]
13. McEver RP, Zhu C. *Annu. Rev. Cell Dev. Biol.* 2010; 26:363. [PubMed: 19575676]
14. Orr FW, Wang HH, Lafrenie RM, Scherbarth S, Nance DM. *J. Pathol.* 2000; 190:310. [PubMed: 10685065]
15. Karnik R, Hong S, Zhang H, Mei Y, Anderson DG, Karp JM, Langer R. *Nano Lett.* 2008; 8:1153. [PubMed: 18321075] Lee C-H, Bose S, Van Vliet KJ, Karp JM, Karnik R. *Langmuir*. 2011; 27:240. [PubMed: 21141947] Nishimura T, Miwa J, Suzuki Y, Kasagi N. *J. Micromech. Microeng.* 2009; 19:125002. Greenberg AW, Hammer DA. *Biotechnol. Bioeng.* 2001; 73:111. [PubMed: 11255159] Chang WC, Lee LP, Liepmann D. *Lab Chip*. 2005; 5:64. [PubMed: 15616742] Mahara A, Yamaoka T. *Biomaterials*. 2010; 31:4231. [PubMed: 20185169] Eddington C, Murata H, Koepsel R, Andersen J, Eom S, Kanade T, Balazs AC, Kolmakov G, Kline C, McKeel D, Liron Z, Russell AJ. *Langmuir*. 2011; 27:15345. [PubMed: 22111791]
16. Choi S, Park J-K. *Lab Chip*. 2007; 7:890. [PubMed: 17594009] Choi S, Park J-K. *Small*. 2009; 5:2205. [PubMed: 19637272]
17. Norman KE, Moore KL, McEver RP, Ley K. *Blood*. 1995; 86:4417. [PubMed: 8541529]
18. Snapp KR, Wagers AJ, Craig R, Stoolman LM, Kansas GS. *Blood*. 1997; 89:896. [PubMed: 9028320]

19. Malý P, Thall AD, Petryniak B, Rogers CE, Smith PL, Marks RM, Kelly RJ, Gersten KM, Cheng G, Saunders TL, Camper SA, Camphausen RT, Sullivan FX, Isogai Y, Hindsgaul O, von Andrian UH, Lowe JB. *Cell*. 1996; 86:643. [PubMed: 8752218]
20. Goldman AJ, Cox RG, Brenner H. *Chem. Eng. Sci.* 1967; 22:653.
21. Inglis DW, Davis JA, Austin RH, Sturm JC. *Lab Chip*. 2006; 6:655. [PubMed: 16652181]
22. Bell GI. *Science*. 1978; 200:618. [PubMed: 347575]

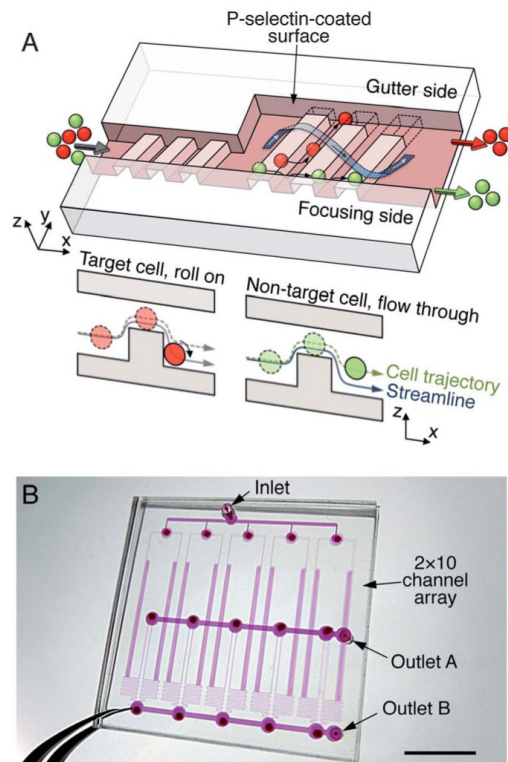


Fig. 1. Scalable parallel sorting device. (A) (Top) Schematic of a single microfluidic channel comprising the focusing ridges in the narrow channel and the sorting ridges in the wide channel. The ribbon indicates a schematic helical streamline. (Bottom) Cross-section views of the wide sorting channel along the x-axis, showing the cell trajectories. (B) The 2×10 channel array is in a 3.5 cm square device. Scale bar, 1 cm.

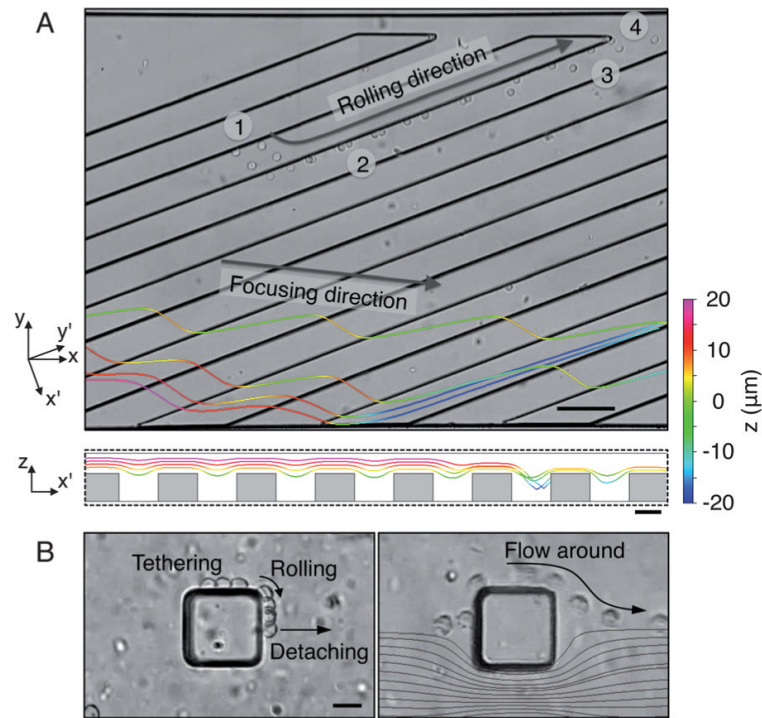


Fig. 2. Deterministic cell rolling. (A) Overlay image showing a rolling sequence of two HL60 cells in order of (1) tethering, (2) rolling on the vertical wall, (3) rolling on the bottom wall, and (4) detaching. The time difference between each frame (total 12 frames) is ~ 6 s. The maximum wall shear stress on the SR was 3.4 dyn/cm^2 . Simulated streamlines over the SR are overlaid on the image; the side view shows the streamlines projected along the SR, y' axis. The top surface of the SR was set to $z = 0 \text{ }\mu\text{m}$. (B) Rolling dynamics on a model square post. (Left) The HL60 cell rolls on the P-selectin-coated post, crossing the streamlines, whereas (Right), the HL60 cell does not bind to the BSA-passivated post and flows along the streamlines. The lines represent simulated streamline paths. The maximum wall shear stress on the post was 3 dyn/cm^2 (channel Reynolds number ~ 0.1). Scale bars, $100 \text{ }\mu\text{m}$ (A) and $20 \text{ }\mu\text{m}$ (B).

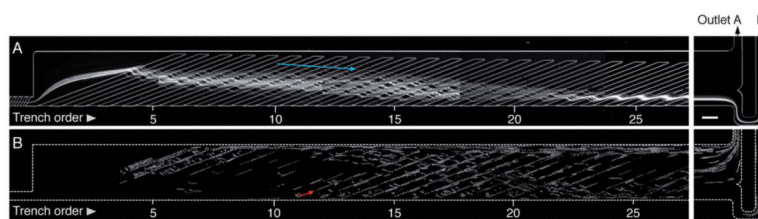


Fig. 3.

Trajectories of HL60 cells in passivated and P-selectin-coated channels. (A) The fluorescently labeled cells are focused into a single stream after passing through the focusing channel. The cell stream that enters the sorting channel is focused again to a tight streamline about 25 ridges downstream. The entire channel was passivated with 1% BSA solution. The arrow indicates the focusing direction of cells. (B) Overlay trajectories of rolling HL60 cells. The time difference between each frame (total 19 frames) is ~ 1.5 s. The entire channel was incubated with P-selectin solution of $1.5 \mu\text{g mL}^{-1}$. The channel geometry is the same as in (A). The arrow indicates the rolling trajectory of a cell. Scale bar, $200 \mu\text{m}$.

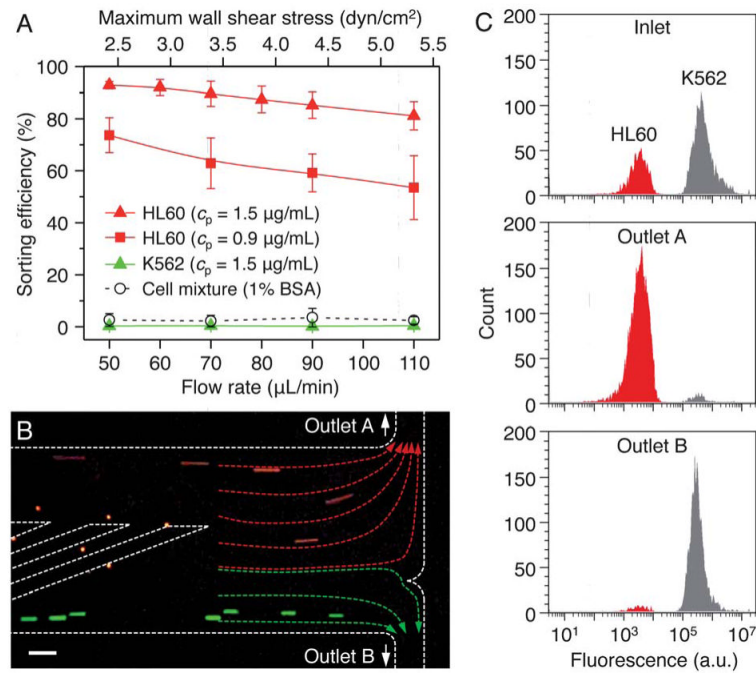


Fig. 4. Parallel sorting of leukemic cell lines. (A) Effect of shear stress (σ) and P-selectin incubation concentration (c_p) on the sorting efficiencies of HL60 and K562 cells for a single sorting channel. As a negative control, the device passivated with 1% BSA solution was tested with the cell mixture of HL60 and K562. Error bars, s.d. ($n = 3$). (B) Sorting of HL60 (red) and K562 (green) cells at $\sigma = 3.4 \text{ dyn/cm}^2$ and $c_p = 1.5 \mu\text{g mL}^{-1}$. The flow distribution is indicated by arrows. (C) Flow cytometric analysis of cell sorting. The initial cell mixture consisted of 39.1% HL60 cells. The output at outlet A comprised $95.0 \pm 2.8\%$ HL60 cells, while that at outlet B comprised $94.3 \pm 0.9\%$ K562 cells. Scale bar, 100 μm .